Cadmium Cation Uptake through Amine and Acid Post -Functionalized Santa Barbara Amorphous Materials; Comprehensive Adsorption Studies

Ehsan Binaeian [a*], Alaleh Esfandyari [b], Peiman Valipour [c], Alireza Hoseinpour Kasgary [c]

Siavash Afrashteh [c]

[a] *Department of Chemical Engineering, Qaemshahr Branch, Islamic Azad University, Qaemshahr, Iran*

[d]*Department of Chemical Engineering, College of Engineering, Mazandaran University of Science and Technology, Babol, Iran*

[c] *Department of Textile, Apparel Engineering and Fashion Mod, Qaemshahr Branch, Islamic Azad University, Qaemshahr, Iran*

Corresponding author. Tel.: +98-9123273466

Corresponding author E-mail addresses: ehsan.binaeian@gmail.com, ehsanbina@fjirsm.ac.cn, e.binaeian@qaemiau.ac.ir (E. Binaeian)

Abstract

In this research, a novel adsorbent, nitrilotriacetic acid anhydride (NTAA) and 3-aminopropyltriethoxysilane (APTES) modified Santa Barbara Amorphous materials (SBA-15) as a mesoporous silica was synthesized and applied for the adsorption of cadmium solution. XRD, TEM, SEM, nitrogen adsorption–desorption isotherms and FTIR analysis were used. The adsorption experiments were performed during batch system containing different concentrations of cadmium solution (60-120 mg/L) in pH range of 2 to 10, adsorbent dosage of 100-600 mg/L with contact time interval of 15 to 120 min. The maximum cadmium removal was achieved at

This article has been accepted for publication and undergone full peer review but has not been through the copyediting, typesetting, pagination and proofreading process which may lead to differences between this version and the Version of Record. Please cite this article as doi: 10.1002/ep.13548

pH 6 with 250 mg/L of adsorbent after 60 min. The proposed mechanisms for the removal and capture of Cd^{+2} ions by adsorbent are electrostatic interactions and chelation. The equilibrium studies prove that the experimental data are compatible with the Langmuir isotherm model well with the maximum adsorption capacity of 500 mg/g. Kinetic and thermodynamic studies also indicate that pseudo-second order kinetic model is the predominant model and the adsorption process is exothermic. This study reveals a high capability of novel nano-adsorbent for the efficient removal of hazardous heavy metal cations and anions from wastewater.

Keywords: SBA-15, 3-Aminopropyltrimethoxysilan, Nitrilotriacetic acid anhydride, Cadmium ions, Adsorption

1. Introduction

The existence of metal ions discharged from industrial effluents in aquatic environments is one of the greatest issues of the environmental organizations. Parallel to consideration on the toxicity effects of heavy metals on the life of human, animals and plants, some strategies and techniques should be designed for the removal of theses pollutants. Among all heavy metals, cadmium (Cd) is known as a toxic metal which is discharged into the environment from effluents of different industries such as metallurgy, lead–zinc mining, electroplating, photography, pigment works, and production of alkaline batteries [1]. Exposure to high doses of cadmium causes both acute and chronic problems on living organisms and makes serious diseases such disorders on the nervous system, kidney, liver and cardio vascular system [2]. Maximum allowable doses of cadmium for human from air and water are about 0.15 and 1 μg/day, respectively [3]. Therefore, cadmium removal

from environmental systems is necessary and even vital [4]. Among many separation techniques including coagulation, ultrafiltration, reverse osmosis, membrane separation, solvent extraction and adsorption which are employed for heavy metal removal [5-8], adsorption process has been considered as a simple and cost-effective method for cadmium removal, with consideration on biological and chemical stability of cadmium as a toxic metal [5-7, 9]. Some complexities and nonlinear manners of variables cause some problems for the adsorption mechanism. To improve and optimize the variables of adsorption process, response surface methodology (RSM) as a suitable method was emerged. This method can combine the statistical and mathematical techniques for optimization. RSM technique also are used to assess the extent of multiple variables effects and their interactions[10]. Modeling and optimization of chromium adsorption onto clay using response surface methodology, artificial neural network [10] and optimization of the adsorption process using RSM technique for Cd^{2+} sorption by dimethylethylenediamine-modified zinc-based MOF (ZIF-8-mmen) [11] were reported as the useful modeling techniques to simulate and to optimize the heavy metal removal process. Nowadays, mesoporous materials such as ordered silicate with distinct characteristics including uniform pore size distribution, high surface area, proper mechanical and thermal stability are applied in various fields like catalysis, drug delivery, medical diagnostics, adsorption process and chromatography [12-13]. Up to now, several investigations on synthesis and application of functionalized mesoporous materials for metal ions removal [14-16] , dyes removal [7, 17-20], organic compounds adsorption [21], drug delivery [12, 22-26] and gas storage [27] have been reported. A new type of well-ordered mesoporous silica was prepared in

the University of California in 1998 and named Santa Barbara Amorphous materials (SBA-15) [28]. SBA-15 has cylindrical pores with uniform diameter which are arranged in hexagonal form. Moreover, pore diameters of SBA-15 varies from 5 to 30 nm so that its thicker wall in comparison with other mesoporous silicate enhances its thermal, mechanical and chemical stability[28]. Modification of mesoporous silicates with various types of organic functional groups such as trimethoxy silane [29-30], graphene oxide [31] and N-(2-hydroxyethyl) salicylaldimine [32] have been carried out for the removal of heavy metals. Amine functionalized mesoporous silicas such as MCM-41, MCM-48, HMS and SBA-15 can adsorb cationic and anionic adsorbates with adjusting solution pH. So, amino functional groups have dual-electronic properties which can take both positive and negative charges to generate electrostatic forces. Also, pair electrons of neutral nitrogen in amino groups structure have been considered as the effective functional groups (basic sites) to interact with cations (acidic sites)[33]. On the other hand, the amine groups can get proton in acidic pH and appear in NH_3^+ form. Therefore, positively charged amino groups can interact with anionic pollutants such as metal ions via electrostatic attraction force. Nitrilotriacetic acid (NTA) with three carboxyl groups and nitrogen with pair electrons exhibits strong chelating feature which is favorable characteristic to bind to metals. NTAA is a liquid anhydride form of NTA which can totally react with the material [34]. Application of NTAA as a modifier, to our knowledge, is very poor in the literatures and only few researches have been reported about NTAA features and applications. In the present study, SBA-15 modified by 3-aminopropyltriethoxysilane (APTES) and NTAA was synthesized (NTAA/SBA-15/NH_2). The performance of synthesized adsorbent for

the removal of cationic pollutants, Cd^{+2}, was investigated. The NH_2/SBA-15/NTAA as a novel adsorbent owing to its different functional groups, is able to adsorb both anionic and cationic components at the same time via electrostatic interactions (protonation of NH_2 to NH_3^+) and chelation (electron pair of nitrogen in nitrilotriacetic acid can make chelation with positive charge of cadmium cations through metal binding). The effects of pH, adsorbent dosage, contact times and cadmium concentration were studied. Also, adsorption thermodynamic, isotherms and kinetics were discussed comprehensively.

2.Materials and Method

Tetraethoxysilane (TEOS), Pluronic copolymer P123 ($EO_{20}PO_{70}EO_{20}$) (Mav = 5800), absolute ethanol, hydrochloric acid (HCl, 37%), N,N-dimethylformamide (DMF), 3-aminopropyltrimethoxysilane (APTES, 97%), acetic anhydride, pyridine and nitrilotriacetic acid (NTA) and cadmium nitrate ($Cd(NO_3)_2$) were purchased from Sigma–Aldrich. Deionized water was used in all experiments.

2.1. Preparation of Santa Barbara amorphous (SBA-15)

SBA-15, as support of the studied adsorbent, was synthesized based on a previously reported procedure [35]. Briefly, 5 g of Pluronic P123 was dissolved in a mixture of 25 g absolute ethanol and 2 g HCl (1 M) and the solution was stirred by magnetic stirrer. Then, 10.4 g TEOS was added with continuous stirring. The phase transition from sol to gel was fulfilled in oven at 40°C for 24 h. The prepared SBA-15 was then calcined in a furnace at 600◦C for 6 h, with a heating rate of 100◦C h^{-1}.

2.2. Preparation of NTAA solution

To prepare NTAA solution, 6 mL pyridine, 6 mL DMF and 4 g NTA were mixed in a 150 mL Erlenmeyer flask. Then, 6 mL acetic anhydride was added dropwise. The solution was stirred at 65 ºC for 24 h to form NTAA.

2.3. Preparation of NH_2/SBA-15/NTAA

To synthesis the composite sample, 1 g SBA-15, 3 ml APTES and 6 ml DMF were added into NTAA solution which was prepared in section 2.2. Then, suspension was stirred at 75ºC for 20 min. After separation of solid samples by filtration, the prepared smple was washed by acetic anhydride, DMF, deionized water, ethanol and acetone, and then was dried at 70ºC for 24 h [36].

2.4. Characterization

Surface morphology of specimens were analyzed by HITACHI S-4160 scanning electron microscopy (SEM). Transmission electron microscopy (TEM) images of SBA-15 and NH_2/SBA-15/NTAA nanocomposites were obtained (TEM, CM120, PHILIPS, Holland, 150kV). X-ray diffraction (XRD) patterns of SBA-15 and NH_2/SBA-15/NTAA in low and high angles were prepared using diffractometer (35kV, 28.5mA and 25°C, Philips instruments, Australia) where copper anode was used as a radioactive source. To demonstrate the presence of nitrilotriacetic acid and amine on the surface of MNPs, Fourier transform infrared spectrometry (FTIR, 8400S, Shimadzu, Japan) in the wave numbers ranging of 400–4000cm^{-1} was applied. The BET surface area was evaluated from the linear part of BET plot. Pore size and pore volume distributions were also estimated from the adsorption curve of N_2 adsorption-desorption isotherm by BJH (Barret–Joyner–Halenda) method (Quanta chrome NovaWin2, USA).

2.5. Batch adsorption procedure

The effect of some basic parameters such as, pH, contact time, initial concentrations of Cd^{+2}, adsorbent dosage and temperature on Cd^{+2} removal were investigated. The effect of pH was investigated in the range of 2 to 10. At optimum pH, adsorbent dosage (100-600 mg/L), adsorption kinetic parameters in different time intervals (15-120 min) were studied. Then, to study the equilibrium state data, the isotherm models were prepared. Finally, the effect of temperature in the range of 25 to 45°C at optimum pH, contact time and dosage were studied and thermodynamic parameters such as Gibbs free energy, enthalpy and entropy were calculated. The equilibrium concentrations of cadmium were calculated using atomic absorption spectrophotometer (Varian Spectra AA220). The removal efficiency and adsorption capacity of Cd^{2+} on NH_2/SBA-15/NTAA were calculated by the following equations [9, 37-38]:

$$\text{Re}\,moval \quad Efficiency = \frac{C_i - C_t}{C_i} \times 100 \tag{1}$$

$$q_t = \frac{(C_i - C_t) \times V}{M} \tag{2}$$

Where q_t (mg/g) is the adsorption capacity at any time *t*, C_o and C_t (mg/L) are initial concentration and equilibrium concentrations at any time *t*, *V* and *M* are volume of cadmium solution (L) and nanocomposite dosage (g), respectively.

3.Results and discussion

3.1. Characterization of SBA-15 and NH_2/SBA-15/NTAA

The N_2 adsorption/desorption isotherms and pore size distribution of SBA-15 and NH_2/SBA-15/NTAA are shown in Fig.1. As seen in Fig. 1a, SBA-15 shows type IV isotherm and a sharp increase in nitrogen adsorption up to P/P_0=0.61 which are the characteristics of ordered mesoporous materials [5, 7, 13, 36]. For NH_2/SBA-15/NTAA, the volume of adsorbed nitrogen decreases accompanied by slight movement of isotherm curve towards lower relative pressure, indicating the reduction of pore size of SBA-15. Also, emerging a hysteresis at around the relative pressure of 0.4 demonstrates the existence of capillary condensation pores [5]. The textural analysis results of material are presented in Table 1. The synthesized SBA-15 with relative high surface area (S_{BET}=537.47m^2/g), pore volume and BJH pore size of 0.29 cm^3/g and 2.40 nm clearly exhibits its meso-structure. Also, Fig. 1b reveals that pore sizes of SBA-15 are in meso region with sharp peak around 2.40 nm. After functionalization of SBA-15 by amine and nitrilotriacetic acid anhydride, specific surface area, pore volume and average pore diameter calculated by BJH method decrease to 165.41 m^2/g, 0.25 cm^3/g and 2.18 nm, respectively. So, these reduced values could be attributed to the partial blockage of SBA-15 pores after functionalization by amine and NTAA.

<<Fig.1>>

<<Table 1>>

SEM and TEM images of SBA-15 and NH_2/SBA-15/NTAA are shown in Fig.2. As seen in Fig. 2 (a,b,c), SBA-15 particles with the same sizes and rod shape (fiber-like) are formed which are similar to the findings of many researches [12, 28]. Also, Fig. 2 (d,e,f) exhibits slight roughness and hardness on SBA-15 surface after functionalization by amine and NTAA. Karimi and coworkers

synthesized acid modified SBA-15 with this characteristics and morphology as a highly sensitive fluorescent probe for detection of Fe^{3+} and I^- ions in water [39]. Fig. 2 (g,h) shows the TEM images of SBA-15 and NH_2/SBA-15/NTAA. The hexagonal structures of SBA-15 (Fig. 2g) and NH_2/SBA-15/NTAA (Fig. 2h) are similar to the TEM images of SBA-15-SB-Mn [40] and SBA-FC-S5-Au [41] which were prepared by Paul and Chen, respectively.

<<Fig.2>>

X-ray diffraction (XRD) patterns of SBA-15 and NH_2/SBA-15 /NTAA in low and high angles and FTIR spectra of SBA-15 and NH_2/SBA-15/NTAA are shown in Fig. 3. For SBA-15 (Fig. 3a), all peaks are compatible with the range of standard spectrum (JCPDS card no. 04-0784). For NH_2/SBA-15/NTAA in low angles region (Fig. 3b), there are two peaks at $2\theta=0.85^{o}$ and $2\theta=1.4^{o}$ which are characteristic of hexagonal and crystalline structure of SBA-15. Also, reflected peak at $2\theta=22^{o}$ for SBA-15 and NH_2/SBA-15/NTAA shows the presence of silica which is attributed to the amorph structure of SBA-15 [42-43]. Moreover, the similar XRD patterns of SBA-15 and NH_2/SBA-15/NTAA shows that the hexagonal and crystalline structure of SBA-15 was not damaged after modification (Fig.3b). The FTIR spectra of SBA-15 (Fig. 3c) shows the broad and wide band at 3449.97 cm^{-1} which is related to the surface hydroxyl groups (Si-OH in SBA-15). Vibration and sharp peak in 1087 cm^{-1} indicates the vibration of Si-O-Si groups (asymmetric stretch). Peaks at 802 cm^{-1} and 465 cm^{-1} reveal the bending stretching and symmetric stretching of Si-O-Si, respectively [27-28, 35, 43]. These peaks also can be seen in FTIR spectrum of NH_2/SBA-15/NTAA, which exhibit the overlap of vibrations of Si-O-Si bonds in SBA-15 and vibrations of

Si-O-Si from silisium in SBA-15 and silisium in aminopropyltriethoxysilane. So, it means that the favorable bond for immobilization of aminopropyl on SBA-15 is formed [42-43]. In the spectrum of NH_2/SBA-15 NTAA, a weak peak around 3000 cm^{-1} is related to stretching of C-H band. The spectrum of NH_2/SBA-15/NTAA also exhibits the peaks related to the bending vibration of N-H around 690 and 1650 cm^{-1} and shear vibration of NH_2 at 1580 cm^{-1}, indicating the existence of amine groups [44-45]. The new peak at 1740 cm^{-1} shows ester bond and carboxyl in SBA-15 structure after functionalization NTAA, that are not existence in the spectrum of pristine SBA-15 [34, 44].

<<Fig.3>>

3.2. Effect of initial pH on adsorption of Cd^{+2}

Fig.4 shows the effect of solution pH on the cadmium removal. As seen, the removal of Cd^{+2} increases with the increase of pH. In lower pHs, amine groups of modified SBA-15 (NH_2) are changed into protonated form, i.e. NH_3^+ similar to hydronium ions (H_3O^+). Therefore, repultion interactions among NH_3^+, H_3O^+ and Cd^{+2} reduces cadmium adsorption performance[36]. Also, increasing pH causes weaker protonation of NH_2/SBA-15/NTAA surface and increase Cd^{+2} uptake. Therefore, both electrostatic interactions and chelation via electron pair of nitrogen in nitrilotriacetic acid and positive charge of cations control cadmium uptake. The neutral surface charge of adsorbent is defined by the zero-point charge (ZPC) concept. In this research the zero-point charge (ZPC) of NH_2/SBA-15/NTAA was calculated about 4. To calculate the zero-point charge (pH_{zpc}) of NH_2/SBA-15/NTAA, NaCl solutions (0.1 M) were prepared with different initial pH range of 2 to 12. pHs were adjusted by 1 M NaOH or H_2SO_4 solutions. Then, 0.05 g of

NH_2/SBA-15/NTAA was added to each solution followed by 48 h stirring. After filtration, the final pH of each solution was recorded. Finally, pH_{pzc} was determined from the intersection of the final curve pH vs. initial pH. At pH below pH_{pzc} of NH_2/SBA-15/NTAA, adsorbent surface gains proton, and NH_3^+ specie of the surface limits cadmium uptake through electrostatic repulsion. At pH equal to the zero-point charge of NH_2/SBA-15/NTAA, surface charge of the adsorbent is zero, i.e. negative and positive surface charges are in balance. Therefore, surface electrostatic interactions such as NH_3^+-NH_3^+ and NH_3^+-Cd^{+2} repulsion interactions are minimized, enhancing cadmium uptake. At pH> pH_{pzc} with increasing negatively surface charges, Cd^{+2} uptake increases by the NH_2/SBA-15/NTAA through both electrostatic interactions and chelation[36]. Maleki and coworkers reported such trend of cadmium uptake for cadmium uptake using amine modified ZIF-8[11]. Moreover, at pH>6, cadmium precipitates in $Cd(OH)_2$ form. So, all experiments were designed for pH values below 6 [15, 36, 46]. In some researches conducted by Moradi and coworkers for lead removal from the aquatic environment using pumice powder [47], by Mansourian and coworkers for the removal of nickel and chromium from aqueous solution using zeolite powder [48] and by Agarwal and coworkers for rapid removal of noxious nickel (II) using novel γ-alumina nanoparticles and multiwalled carbon nanotubes [49], the effect of pH on the adsorption of heavy metals were discussed.

<<Fig.4>>

3.3. Effect of contact time

To evaluate the equilibrium state of adsorption, Cd^{+2} adsorption on NH_2/SBA-15/NTAA was performed for 120 min with different time interval. For all cadmium concentrations and after 60 min contact time, the adsorption was completed and equilibrium state was achieved (Fig.5). In fact, after 60 min, the maximum cadmium uptake is rapidly obtained [49]. Due to plentiful active sites, cadmium uptake was completed fast during the early steps of the adsorption. But, with slight decrease of active sites, cadmium uptake was restricted with slower rate. On the other word, accumulation of cadmium on NH_2/SBA-15/NTAA with the increasing time, prevents the deeper diffusion of cadmium into the active sites of adsorbent with higher energy [15, 36, 46].

<<Fig.5>>

3.4. Effect of initial cadmium concentration

experiments were conducted with different concentrations of cadmium solution (20 to 120 mg/L). Increasing concentration up to 60 mg/L caused the increase of cadmium adsorption. Increasing concentration more than 60 mg/L decreases the cadmium removal efficiency (Fig.6) [50-51]. In fact, the existence of mass transfer resistance among solid-liquid phase is adjusted by driving force which is provided by initial concentration. But, with the increase of initial cadmium concentration at constant NH_2/SBA-15/NTAA dosage, mass transfer resistance increases, while the numbers of active sites remain constant. Therefore, cadmium uptake decreases due to lower access to NH_2/SBA-15/NTAA surface[7, 46].

<<Fig.6>>

3.5. Effect of temperature and thermodynamic study

Thermodynamic parameters including Gibbs free energy (ΔG), enthalpy (ΔH) and entropy (ΔS) were calculated at 25 to 45°C using following equations [52-54]:

$$k_c = C_{Ae} / C_e \quad (3)$$

$$\Delta G^o = -RT \ln k_c \quad (4)$$

$$\log k_c = (\Delta S^o / 2.030R) - \Delta H^o / 2.303RT \quad (5)$$

The results show that increasing temperature decreases the removal percentage of Cd^{+2} from 96.62% to 81.90%. So, cadmium adsorption is exothermic. The exothermic adsorption process is inhibited with rising temperatures. The feasibility and spontaneous nature of the adsorption process is assessed using Gibbs free energy (ΔG) which is calculated from Eq. (4). The negative value of ΔH (-55.31 kJ/mol) shows the exothermic nature of the adsorption process. Several authors also verified exothermic adsorption of Cd^{+2} on calcium treated bentonite clay [55], cadmium ions adsorption using guanine-functionalized mesoporous silica [SBA-16-g] [56] and removal of cadmium from aqueous solutions by adsorption onto polyethylenimine-functionalized mesocellular silica foam [57]. Absolute high value of ΔH (>40 kJ/mol) proves the chemisorption of Cd^{+2} onto the NH_2/SBA-15/NTAA[52-54]. The spontaneity of the process at the liquid-solid interface is evaluated by positive entropy change (ΔS) so that the positive value of entropy (0.162 kJ/mol) represents the increase of irregularity and increasing efficiency over the time [58-59]. The negative values of ΔG at three temperatures (-3.13, -2.08, -1.73 kJ/mol) exhibit the feasible and spontaneous adsorption process. The feasibility and spontaneity of the cadmium adsorption is restricted by increasing temperature which is in agreement with exothermic nature of this process [58, 60].

3.6. Isotherms of Cd^{+2} adsorption on NH_2/SBA-15/NTAA

The N_2 isotherm data were collected after contact of 100 mL cadmium solutions (60 to 120 mg/L) with NH_2/SBA-15/NTAA (250 mg/L) for 60 min. Four types of isotherm models including Langmuir, Freundlich, Dubinin-Radushkevich and Temkin were prepared. The results are listed in Table 2 and shown in Fig 7. As seen, the Langmuir model is more compatible with the experimental results and R^2 values (0.94) is near to unity in comparison with other isotherm models. So, mono-layer adsorption of cadmium occurred on H_2/SBA-15/NTAA with uniform and homogeneously distribution of acceptor groups. Also, maximum mono-layer uptake capacity calculated by Langmuir model ($q_{cal.}$=500 mg/g) is higher than that of experimental value ($q_{exp.}$=128 mg/g). So, adsorption is monolayer and surface is not covered completely by cadmium [61]. For the adsorption of Cd^{2+} from aqueous systems by SDS modified mesoporous silica MCM-41 [62], adsorption of cadmium from aqueous solution using Enteromorpha prolifera biochar modified with different chemical reagents [63] and cadmium adsorption using guanine-functionalized mesoporous silica [SBA-16-g] [56], Langmuir isotherm was the predominant isotherm model between other isotherm models. The Freundlich isotherm assumes multilayer adsorption on the heterogeneous surface of adsorbent. From the Freundlich isotherm, *n* value was obtained about 3.74, illustrating the favorable adsorption. The correlation coefficient of Temkin model (R^2=0.80) is less than those of Langmuir (R^2=0.94) and Freundlich (R^2=0.87) models. So, it does not justify multi-layer adsorption, indicating monolayer adsorption of cadmium on specific homogeneous site [56]. The interactions between adsorbate and adsorbent can be evaluated via mean free energy of adsorption,

E, which is calculated using the Dubinin-Radushkevich (D–R) isotherm model.For E <8 kJ mol^{-1}, adsorption process is involved via physical interactions, while the chemical interactions are emerged when 8<E <16 kJ/mol [62]. The value of *E* calculated by D-R model is higher than 8 kJ/mol (8.99 kJ/mol) representative of the chemisorption of cadmium on NH_2/SBA-15/NTAA [6, 64]. The results of some researches for Cd(II) adsorption on Enteromorpha prolifera biochar modified with different chemical reagents [63] and cadmium uptake on polyacrylic acid-based and chitosan-based hydrogels [65] proved that the chemical adsorption is the controlling step for the cadmium adsorption process.

<<Table 2>>
<<Fig.7>>

For comparative purposes, the adsorption capacity of cadmium adsorption onto different adsorbents is listed in Table 3. With the comparison of maximum adsorption capacity of cadmium (q_m), it is seen that NH_2/SBA-15/NTAA with amine and NTAA, exhibits favorable adsorption. .

<<Table 3>>

3.7. Adsorption kinetics

The adsorption kinetic models are employed to understand the mechanism and rate of adsorption onto the adsorbent. Three kinetic models including pseudo-first order, pseudo-second order and intra-particle diffusion model (Weber and Morris model) were applied as beolow[5-7, 43-44]:

$$\ln(q_e - q_t) = \ln(q_e) - k_1 t \quad (6)$$

$$\frac{t}{q_t} = \frac{1}{k_2 q_e^2} + \frac{t}{q_e} \quad (7)$$

$$q_t = k_p t^{0.5} + C \quad (8)$$

Where q_t (mg/g) and q_e (mg/g) are adsorption capacities at time t and at equilibrium, respectively. k_1 (min^{-1}), k_2 ($g.mg^{-1}\ min^{-1}$), k_p ($mg.g^{-1}\ .min^{-0.5}$) and C are the kinetic rate constants or the pseudo-first-order, the pseudo-second-order model, intraparticle diffusion rate constant and the boundary layer effects, respectively [53, 64]. The results are shown in Table 4. This Table contains kinetic parameters and correlation coefficients (R^2). Table 4 show that the adsorption capacities calculated by pseudo-second order model ($q_{e,cal}$) in comparison with pseudo-first order kinetic model, are more compatible with experimental data ($q_{e,exp}$). So, the adsorption of cadmium is followed by the pseudo-second-order kinetic model, and the assumption of rate controlling by chemical sorption is satisfied. Cadmium removal from aqueous solution using guanine-functionalized mesoporous silica [SBA-16-g] [56], the adsorption of cadmium ions (Cd (II)) from the synthesis wastewater with the activated carbon [66] and cadmium (II) ions adsorption from water by amino modification of rice straw-derived biochar [67] are some adsorption process that pseudo-second order kinetic model are the predominant kinetic model during cadmium adsorption. A linear form of intra-particle diffusion model is divided into two straight lines indicating boundary layer effects and metal ion penetration into the pores of the adsorbent which is co-called the intra-particle diffusion[56]. The linear graphs do not pass through the origin and the intra-particle diffusion is not the only rate-controlling step. Boundary layer effects increase with the increase of the Cd^{+2} initial concentration. So, adsorption kinetic is controlled by film and pore diffusion combination [63, 66]. The values of k_p and C from intra-particle model were calculated and listed in Table 4.

<<Table 4>>

3.8. Desorption and reusability studies

The regeneration performance of an adsorbent is very important for the large-scale application. For reusing adsorbent, adsorbed components should be easily desorbed under moderate conditions. To achieve this aim, desorption of adsorbed cadmium from NH_2/SBA-15/NTAA was carried out via batch system with HCl (0.1 M) for 4h. The reusability of NH_2/SBA-15/NTAA was evaluated over six consecutive cycles with 25 mg adsorbent in 100 mL cadmium solution (60 mg/L) at 25^oC for 60 min (each cycle). The results of regeneration tests are shown in Fig. 8. As seen, after six cycles of reusability tests, the adsorption capacity of cadmium on adsorbent changed slightly so that only 7.33% reduction in efficiency of NH_2/SBA-15/NTAA was observed. Therefore, NH_2/SBA-15/NTAA can be regenerated easily using HCl solution with repeated usability. This is a promising characteristic of each efficient adsorbent for the practical wastewater treatment.

<<Fig.8>>

4.Conclusion

In the present research, nitrilotriacetic acid anhydride (NTAA) and 3-aminopropyltriethoxysilane (APTES) were introduced into the as-synthesized SBA-15, through two steps of acidification and amination. After modification of SBA-15 for cadmium removal tests, specific surface area of SBA-15 decreased from 537 to 165 m^2/g, indicating the loading of SBA-15 by functional groups that may cause the partial blockage of the pores and decreasing nitrogen adsorption. The maximum Cd^{+2} adsorption was achieved at pH 6 with 250 mg/L adsorbent in 60 mg/L cadmium solution. It

was proved that in acidic range, amine groups (NH_2) which are existing in the structure of NH_2/SBA-15/NTAA, changed into NH_3^+ form in associated with hydronium ions (H_3O^+). So, these cations limit Cd^{+2} adsorption due to repulsion forces. With the enhancement of pH, weaker protonation of composite surface leads to the increase of Cd^{+2} adsorption. So, Cd^{+2} could be adsorbed by the NH_2/SBA-15/NTAA through electrostatic interactions and chelation (electrons of NTAA and positive charge of cadmium cations). Rising temperatures inhibited the performance of cadmium adsorption (25 to 45ºC). Equilibrium and kinetic studies demonstrated that the Langmuir isotherm with maximum adsorption capacity of 500 mg/g and pseudo-second order kinetic model are compatible with the experimental data. So, monolayer adsorption of cadmium occurred on humogen surface of adsorbent via chemical interaction. Also, the enthalpy of adsorption was calculated -55.31 kJ/mol. The negative values of enthalpy and Gibbs free energy indicate that the adsorption process is exothermic and spontaneous. Desorption and reusability studies exhibited that after six cycles of reusability, 7.33 % reduction in efficiency of NH_2/SBA-15/NTAA was observed, indicating repeatedly application of NH_2/SBA-15/NTAA adsorbent for practical wastewater treatment. The results of this study proved that the new synthesized NH_2/SBA-15/NTAA nano-adsorbent is an efficient adsorbent for the purifications and separation in many fields of chemical engineering, where this adsorbent with its dual functional groups is so useful for the adsorption of both cation and anion agents in various ranges of pH.

5. Acknowledgments

Authors gratefully acknowledge the supports from the qaemshahr branch, islamic azad university and college of engineering, Mazandaran university of science and technology, babol.

References

1. Lee, S. M.; Laldawngliana, C.; Tiwari, D., Iron Oxide Nano-Particles-Immobilized Sand Material in the Treatment of Cu(II), Cd(II) and Pb(II) Contaminated Waste Waters. *Chemical Engineering Journal* **2012,** *195-196*, 103-111.
2. Tang, W. W.; Zeng, G. M.; Gong, J. L.; Liang, J.; Xu, P.; Zhang, C.; Huang, B. B., Impact of Humic/Fulvic Acid on the Removal of Heavy Metals from Aqueous Solutions Using Nanomaterials: a Review. *Science of the Total Environment* **2014,** *468*, 1014–1027.
3. Hajiaghababaei, L.; Badiei, A.; Ganjali, M. R.; Heydari, S.; Khaniani, Y.; Ziarani, G. M., Highly Efficient Removal and Preconcentration of Lead and Cadmium Cations from Water and Wastewater Samples Using Ethylenediamine Functionalized SBA-15. *Desalination* **2011,** *266*, 182–187.
4. Khan, T. A.; Singh, V. V., Removal of Cadmium(II), Lead(II), and Chromium(VI) Ions from Aqueous Solution Using Clay. *Toxicological & Environmental Chemistry* **2010,** *92*, 1435–1446.
5. Hadizade, G.; Binaeian, E.; Emami, M. R. S., Preparation and Characterization of Hexagonal Mesoporous Silica/Polyacrylamide Nanocomposite Capsule (PAM-HMS) for Dye Removal from Aqueous Solutions. *Journal of Molecular Liquids* **2017,** *238*, 499–507.
6. Shabandokht, M.; Binaeian, E.; Tayebi, H. A., Adsorption of Food Dye Acid Red 18 onto Polyaniline-Modified Rice Husk Composite: Isotherm and Kinetic Analysis. *Desalination and Water Treatment* **2016,** *57*, 27638-27650.
7. Binaeian, E.; Tayebi, H. A.; Rad, A. S.; Afrashteh, S., Adsorption of Acid Blue on Synthesized Polymeric Nanocomposites, PPy/MCM-41 and PAni/MCM-41: Isotherm, Thermodynamic and Kinetic Studies. *Journal of Macromolecular Science, Part A* **2018,** *55*, 269–279.

8. Khan, T. A.; Nazir, M.; Khan, E. A.; Riaz, U., Multiwalled Carbon Nanotube–Polyurethane (MWCNT/PU) Composite Adsorbent for Safranin T and Pb(II) Removal from Aqueous Solution: Batch and Fixed-Bed Studies. *Journal of Molecular Liquids* **2015,** *212*, 467-479.
9. Khan, T. A.; Nazir, M.; Khan, E. A., Magnetically Modified Multiwalled Carbon Nanotubes for the Adsorption of Bismarck Brown R and Cd(II) from Aqueous Solution: Batch and Column Studies. *Desalination and Water Treatment* **2016,** *57*, 19374-19390
10. Oskui, F. N.; Aghdasinia, H.; Sorkhabi, M. G., Modeling and optimization of chromium adsorption onto clay using response surface methodology, artificial neural network, and equilibrium isotherm models. *Environmental Progress & Sustainable Energy* **2019,** *38* (6), e13260.
11. Binaeian, E.; Maleki, S.; Motaghedi, N.; Arjmandi, M., Study on the performance of Cd2+ sorption using dimethylethylenediamine-modified zinc-based MOF (ZIF-8-mmen): optimization of the process by RSM technique. *Separation Science and Technology* **2019**, 1-16.
12. Legnoverde, M. S.; Basaldella, E. I., Influence of Particle Size on the Adsorption and Release of Cephalexin Encapsulated in Mesoporous Silica SBA-15. *Materials Letters* **2016,** *181*, 331–334.
13. Majda, D.; Napruszewska, B. D.; Zimowska, M.; Makowski, W., Porosity of SBA-15 After Functionalization of the Surface with Aminosilanes. *Microporous and Mesoporous Materials* **2016,** *234*, 98-106.
14. Bai, L.; Duan, S.; Jiang, W.; Liu, M.; Wang, S.; Sang, M.; Gong, X.; Li, J.; Xuan, S., High Performance Polydopamine-Functionalized Mesoporous Silica Nanospheres for U(VI) Removal. *Applied Surface Science* **2017,** *426*, 1121-1132.
15. Lalchhingpuii; Tiwari, D.; Lalhmunsiama; Lee, S. M., Chitosan Templated Synthesis of Mesoporous Silica and its Application in the Treatment of Aqueous Solutions Contaminated with Cadmium(II) and Lead(II). *Chemical Engineering Journal* **2017,** *328*, 434–444.
16. Kim, J. H.; Kang, J. K.; Lee, S. C.; Kim, S. B., Synthesis of Powdered and Granular N -(3-Trimethoxysilylpropyl) Diethylenetriamine-Grafted Mesoporous Silica SBA-15 for Cr(VI) Removal from Industrial Wastewater. *Journal of Taiwan Institute Chemical Engineering* **2018,** *87*, 140-149.
17. Binaeian, E.; Seghatoleslami, N.; Chaichi, M. J., Synthesis of Oak Gall Tannin-Immobilized Hexagonal Mesoporous Silicate (OGT-HMS) as New Super Adsorbent for the Removal of Anionic Dye from Aqueous Solution. *Desalination and Water Treatment* **2016,** *57*, 8420–8436.
18. Anbia, M.; Salehi, S., Removal of Acid Dyes from Aqueous Mediab Adsorption onto Amino-Functionalized Nanoporous Silica SBA-3. *Dyes and Pigments* **2012,** *94*, 1-9.
19. Zarezadeh-Mehrizi, M.; Badiei, A.; Mehrabadi, A. R., Ionic Liquid Functionalized Nanoporous Silica for Removal of Anionic Dye. *Journal of Molecular Liquids* **2013,** *180*, 95-100.
20. Soltani, R. D. C.; Khataee, A. R.; Safari, M.; Joo, S. W., Preparation of Bio-Silica/Chitosan Nanocomposite for Adsorption of a Textile Dye in Aqueous Solutions. *International Biodeterioration & Biodegradation* **2013,** *85*, 383-391.
21. Russo, P. A.; Carrott, M. M. L. R.; Carrott, P. J. M., Trends in the Condensation/Evaporation and Adsorption Enthalpies of Volatile Organic Compounds on Mesoporous Silica Materials. *Microporous and Mesoporous Materials* **2012,** *151*, 223–230.
22. Xing, R.; Lin, H.; Jiang, P.; Qu, F., Biofunctional Mesoporous Silica Nanoparticles for Magnetically Oriented Target and pH-Responsive Controlled Release of Ibuprofen. *Colloids and Surfaces A: Physicochemical and Engineering Aspects* **2012,** *403*, 7-14.

23. Li, D.; Zhu, Y.; Liang, Z., Alendronate Functionalized Mesoporous Hydroxyapatite Nanoparticles for Drug Delivery. *Materials Research Bulletin* **2013,** *48*, 2201–2204.
24. Bhattacharyya, S.; Wang, H.; Ducheyne, P., Polymer-Coated Mesoporous Silica Nanoparticles for the Controlled Release of Macromolecules. *Acta Biomaterialia* **2012,** *8*, 3429–3435.
25. Popova, M.; Szegedi, A.; Yoncheva, K.; Konstantinov, S.; Petrova, G. P.; Aleksandrov, H. A.; Vayssilov, G. N.; Shestakova, P., New Method for Preparation of Delivery Systems of Poorly Soluble Drugs on the Basis of Functionalized Mesoporous MCM-41 Nanoparticles. *Microporous and Mesoporous Materials* **2014,** *198*, 247–255.
26. Szegedi, A.; Popova, M.; Goshev, I.; Klebert, S.; Mihaly, J., Controlled Drug Release on Amine Functionalized Spherical MCM-41. *Journal of Solid State Chemistry* **2012,** *194*, 257–263.
27. Sanz, R.; Calleja, G.; Arencibia, A.; Sanz-Perez, E. S., Amino Functionalized Mesostructured SBA-15 Silica for CO_2 Capture: Exploring the Relation Between the Adsorption Capacity and the Distribution of Amino Groups by Tem. *Microporous and Mesoporous Materials* **2012,** *158*, 309–317.
28. Santos, S. M. L.; Cecilia, J. A.; Vilarrasa-Garcia, E.; Junior, I. J. S.; Rodríguez-Castellon, E.; Azevedo, D. C. S., The Effect of Structure Modifying Agents in the SBA-15 for its Application in the Biomolecules Adsorption. *Microporous and Mesoporous Materials* **2016,** *232*, 53-64.
29. Melendez-Ortiz, H. I.; Perera-Mercado, Y.; Mercado-Silva, J. A.; Y.Olivares-Maldonado; Castruita, G.; Garcia-Cerda, L. A., Functionalization with Amine-Containing Organosilane of Mesoporous Silica MCM-41 and MCM-48 Obtained at Room Temperature. *Ceramics International* **2014,** *40*, 9701–9707.
30. Bao, Y. X.; Yan, X. M.; Du, W.; Pan, Z. Q.; Zhou, J. L.; Li, L. S., Application of Amine-Functionalized MCM-41 Modified Ultrafiltration Membrane to Remove Chromium (VI) and Copper (II).

. *Chemical Engineering Journal* **2015,** *281*, 460–467.
31. Wang, X.; Pei, Y.; Lu, M.; Lu, X.; Du, X., Highly Efficient Adsorption of Heavy Metals from Wastewaters by Graphene Oxide-Ordered Mesoporous Silica Materials. *Journal of Materials Science* **2015,** *50*, 2113–2121.
32. Tadjarodi, A.; Jalalat, V.; Zare-Dorabei, R., Adsorption of La (III) in Aqueoussystems by N-(2-Hydroxyethyl) Salicylaldimine-Functionalized Mesoporous Silica. *Materials Research Bulletin* **2015,** *61*, 113–119.
33. Dindar, M. H.; Yaftian, M. R.; Rostamnia, S., Potential of Functionalized SBA-15 Mesoporous Materials for Decontamination of Water Solutions from Cr(VI), As(V) and Hg(II) Ions. *Journal of Environmental Chemical Engineering* **2015,** *3*, 986-995.
34. Huang, Y.; Yang, C.; Sun, Z.; Zeng, G.; He, H., Removal of Cadmium and Lead from Aqueous Solutions Using Nitrilotriacetic Acid Anhydride Modified Ligno-Cellulosic Material. *Royal Society of Chemistry* **2015,** *5*, 11475–11484.
35. Dolatyari, L.; Yaftian, M. R.; Rostamnia, S., Removal of Uranium(VI) Ions ftom Aqueous Solutions Using Schiff Base Functionalized SBA-15 Mesoporous Silica Materials. *Journal of Environmental Management* **2016,** *169*, 8-17.
36. Chen, F.; Hong, M.; You, W.; Li, C.; Yu, Y., Simultaneous Efficient Adsorption of Pb^{2+} and MnO_4^- Ions by MCM-41 Functionalized with Amine and Nitrilotriacetic Acid Anhydride. *Applied Surface Science* **2015,** *357*, 856–865.

37. Khan, T. A.; Rahman, R.; Khan, E. A., Decolorization of Bismarck Brown R and Crystal Violet in Liquid Phase Using Modified Pea Peels: Non-Linear Isotherm and Kinetics Modeling. *Modeling Earth Systems and Environment* **2016,** *2*, 141-151.
38. Siddiqui, M. F.; Khan, E. A.; Khan, T. A., Synthesis of MoO3/Polypyrrole Nanocomposite and its Adsorptive Properties Toward Cadmium(II) and Nile Blue from Aqueous Solution: Equilibrium Isotherm and Kinetics Modeling. *Environmental Progress & Sustainable Energy* **2019,** *38*, 1-12.
39. Karimi, M.; Badiei, A.; Lashgari, N.; Mohammadi Ziarani, G., A chromotropic acid modified SBA-15 as a highly sensitive fluorescent probe for determination of Fe3+ and I− ions in water. *Journal of Porous Materials* **2018,** *25* (1), 137-146.
40. Paul, L.; Banerjee, B.; Bhaumik, A.; Ali, M., Catecholase activity of a manganese Schiff base complex functionalized over SBA-15 in aqueous heterogeneous medium. *Microporous and Mesoporous Materials* **2017,** *249*, 78-87.
41. Chen, T.; Chen, B.-T.; Bukhryakov, K. V.; Rodionov, V. O., Thiols make for better catalysts: Au nanoparticles supported on functional SBA-15 for catalysis of Ullmann-type homocouplings. *Chemical Communications* **2017,** *53* (85), 11638-11641.
42. Yu, L.; Yang, X.; Wang, D., TiO_2 Incorporated in Magnetic Mesoporous SBA-15 by a Facile Inner-Pore Hydrolysis Process Toward Enhanced Adsorption–Photocatalysis Performances for As(III). *Journal of Colloid and Interface Science* **2015,** *448*, 525–532.
43. Shafiabadi, M.; Dashti, A.; Tayebi, H. A., Removal of Hg (II) from Aqueous Solution Using Polypyrrole/SBA-15 Nanocomposite: Experimental and Modeling. *Synthetic Metals* **2016,** *212*, 154-160.
44. Li, L.; Wang, X.; Zhang, D.; Guo, R.; Du, X., Excellent Adsorption of Ultraviolet Filters Using silylated MCM-41 Mesoporous Materials as Adsorbent. *Applied Surface Science* **2015,** *328*, 26–33.
45. Hao, S.; Chang, H.; Xiao, Q.; Zhong, Y.; Zhu, W., One-Pot Synthesis and CO_2 Adsorption Properties of Ordered Mesoporous SBA-15 Materials Functionalized with APTMS. *Journal of Physical Chemistry C* **2011,** *115*, 12873–12882.
46. Peer, F. E.; Bahramifar, N.; Younesi, H., Removal of Cd (II), Pb (II) and Cu (II) Ions from Aqueous Solution by Polyamidoamine Dendrimer Grafted Magnetic Graphene Oxide Nanosheets. *Journal of Taiwan Institute Chemical Engineering* **2018,** *87*, 225-240.
47. Moradi, M.; Soltanian, M.; Pirsaheb, M.; Sharafi, K.; Soltanian, S.; Mozafari, A., The Efficiency Study of Pumice Powder to Lead Removal from the Aquatic Environment: Isotherms and Kinetics of the Reaction. *J-Mazand-Univ-Med-Sci* **2014,** *23* (1), 65-75.
48. Mansourian, N.; Javedan, G.; Darvishmotevalli, M.; Sharafi, K.; Ghaffari, H. R.; Sharafi, H.; Arfaeinia, H.; Moradi, M. In *Efficiency evaluation of zeolite powder, as an adsorbent for the removal of nickel and chromium from aqueous solution: Isotherm and kinetic study*, 2016.
49. Agarwal, S.; Tyagi, I.; Gupta, V. K.; Dehghani, M. H.; Jaafari, J.; Balarak, D.; Asif, M., Rapid removal of noxious nickel (II) using novel γ-alumina nanoparticles and multiwalled carbon nanotubes: Kinetic and isotherm studies. *Journal of Molecular Liquids* **2016,** *224*, 618-623.
50. Honarmandrad, Z.; Javid, N.; Malakootian, M., Efficiency of ozonation process with calcium peroxide in removing heavy metals (Pb, Cu, Zn, Ni, Cd) from aqueous solutions. *SN Applied Sciences* **2020,** *2* (4), 703.

51. Farsi, A.; Javid, N.; Malakootian, M., Investigation of adsorption efficiency of Cu2+ and Zn2+ by red soil and activated bentonite from acid copper mine drainage. *Desalination and Water Treatment* **2019,** *144*, 172-184.
52. Zeng, G.; Tang, Y. L. L.; Yang, G.; Pang, Y.; Zhang, Y.; Zhou, Y.; Li, Z.; Li, M.; Lai, M.; He, X.; He, Y., Enhancement of Cd(II) Adsorption by Polyacrylic Acid Modified Magnetic Mesoporous Carbon. *Chemical Engineering Journal* **2015,** *259*, 153–160.
53. Wu, Y.; Qi, H.; Li, B.; Huang, Z.; Li, W.; Liu, S., Novel Hydrophobic Cotton Fibers Adsorbent for the Removal of Nitrobenzene in Aqueous Solution. . *Carbohydrate Polymers* **2017,** *155*, 294–302.
54. Debnath, S.; Ballav, N.; Maity, A.; Pillay, K., Competitive Adsorption of Ternary Dye Mixture Using Pine Cone Powder Modified with β-Cyclodextrin. . *Journal of Molecular Liquids* **2016,** *225*, 679-688.
55. Meneguin, J. G.; Moisés, M. P.; Karchiyappan, T.; Faria, S. H. B.; Gimenes, M. L.; de Barros, M. A. S. D.; Venkatachalam, S., Preparation and characterization of calcium treated bentonite clay and its application for the removal of lead and cadmium ions: Adsorption and thermodynamic modeling. *Process Safety and Environmental Protection* **2017,** *111*, 244-252.
56. Gupta, R.; Gupta, S. K.; Pathak, D. D., Selective adsorption of toxic heavy metal ions using guanine-functionalized mesoporous silica [SBA-16-g] from aqueous solution. *Microporous and Mesoporous Materials* **2019,** *288*, 109577.
57. Snoussi, Y.; Abderrabba, M.; Sayari, A., Removal of cadmium from aqueous solutions by adsorption onto polyethylenimine-functionalized mesocellular silica foam: Equilibrium properties. *Journal of the Taiwan Institute of Chemical Engineers* **2016,** *66*, 372-378.
58. Betiha, M. A.; Moustafa, Y. M.; El-Shahat, M. F.; Rafik, E., Polyvinylpyrrolidone-Aminopropyl-SBA-15 schiff Base hybrid for efficient removal of divalent heavy metal cations from wastewater. *Journal of Hazardous Materials* **2020,** *397*, 122675.
59. Javid, N.; Nasiri, A.; Malakootian, M., Removal of nonylphenol from aqueous solutions using carbonized date pits modified with ZnO nanoparticles. *Desalination and Water Treatment* **2019,** *141*, 140-148.
60. Javid, N.; Malakootian, M., Removal of bisphenol A from aqueous solutions by modified-carbonized date pits by ZnO nano-particles. *Desalination and Water Treatment* **2017,** *95*, 144-151.
61. Oskui, F. N.; Aghdasinia, H.; Sorkhabi, M. G., Adsorption of Cr (III) using an Iranian natural nanoclay: applicable to tannery wastewater: equilibrium, kinetic, and thermodynamic. *Environmental Earth Sciences* **2019,** *78* (4), 106.
62. Kaewprachum, W.; Wongsakulphasatch, S.; Kiatkittipong, W.; Striolo, A.; Cheng, C. K.; Assabumrungrat, S., SDS modified mesoporous silica MCM-41 for the adsorption of Cu2+, Cd2+, Zn2+ from aqueous systems. *Journal of Environmental Chemical Engineering* **2020,** *8* (1), 102920.
63. Li, X.; Wang, C.; Tian, J.; Liu, J.; Chen, G., Comparison of adsorption properties for cadmium removal from aqueous solution by Enteromorpha prolifera biochar modified with different chemical reagents. *Environmental Research* **2020,** *186*, 109502.
64. Tsai, C. H.; Chang, W. C.; Saikia, D.; Wu, C. E.; Kao, H. M., Functionalization of Cubic Mesoporous Silica SBA-16 with Carboxylic Acid via One-Pot Synthesis Route for Effective Removal of Cationic Dyes. . *Journal of Hazardous Materials* **2015,** *309*, 236-248.

65. Vilela, P. B.; Matias, C. A.; Dalalibera, A.; Becegato, V. A.; Paulino, A. T., Polyacrylic acid-based and chitosan-based hydrogels for adsorption of cadmium: Equilibrium isotherm, kinetic and thermodynamic studies. *Journal of Environmental Chemical Engineering* **2019,** *7* (5), 103327.
66. Kavand, M.; Eslami, P.; Razeh, L., The adsorption of cadmium and lead ions from the synthesis wastewater with the activated carbon: Optimization of the single and binary systems. *Journal of Water Process Engineering* **2020,** *34*, 101151.
67. Zhang, Y.; Yue, X.; Xu, W.; Zhang, H.; Li, F., Amino modification of rice straw-derived biochar for enhancing its cadmium (II) ions adsorption from water. *Journal of Hazardous Materials* **2019,** *379*, 120783.
68. Saeed, A.; Iqbal, M.; Höll, W. H., Kinetics, Equilibrium and mechanism of Cd^{+2} Removal from Aqueous Solution by Mungbean Husk. *Journal of Hazardous Materials* **2009,** *2*, 1467–1475.
69. Zhang, Z.; Li, M.; Chen, W.; Zhu, S.; Liu, N.; Zhu, L., Immobilization of Lead and Cadmium from Aqueous Solution and Contaminated Sediment Using Nanohydroxyapatite. *Environmental Pollution* **2010,** *158*, 514–519.
70. Qu, Q.; Gu, Q.; Gu, Z.; Shen, Y.; Wang, C.; Hu, X., Efficient Removal of Heavy Metal from aqueous Solution by Sulfonic Acid Functionalized Nonporous Silica Microspheres. *Colloids and Surfaces A: Physicochemical and Engineering Aspects* **2012,** *415*, 41-46.

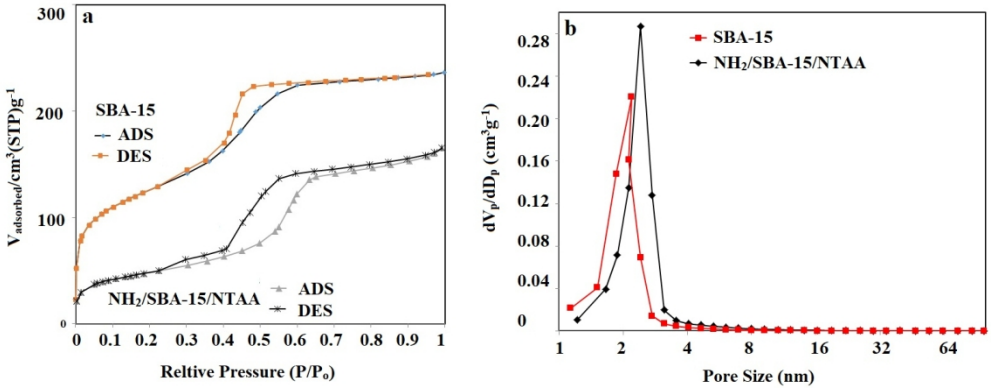

Fig. 1. N2 adsorption–desorption isotherms, pore size distribution of SBA-15 and NH2/SBA-15/NTAA

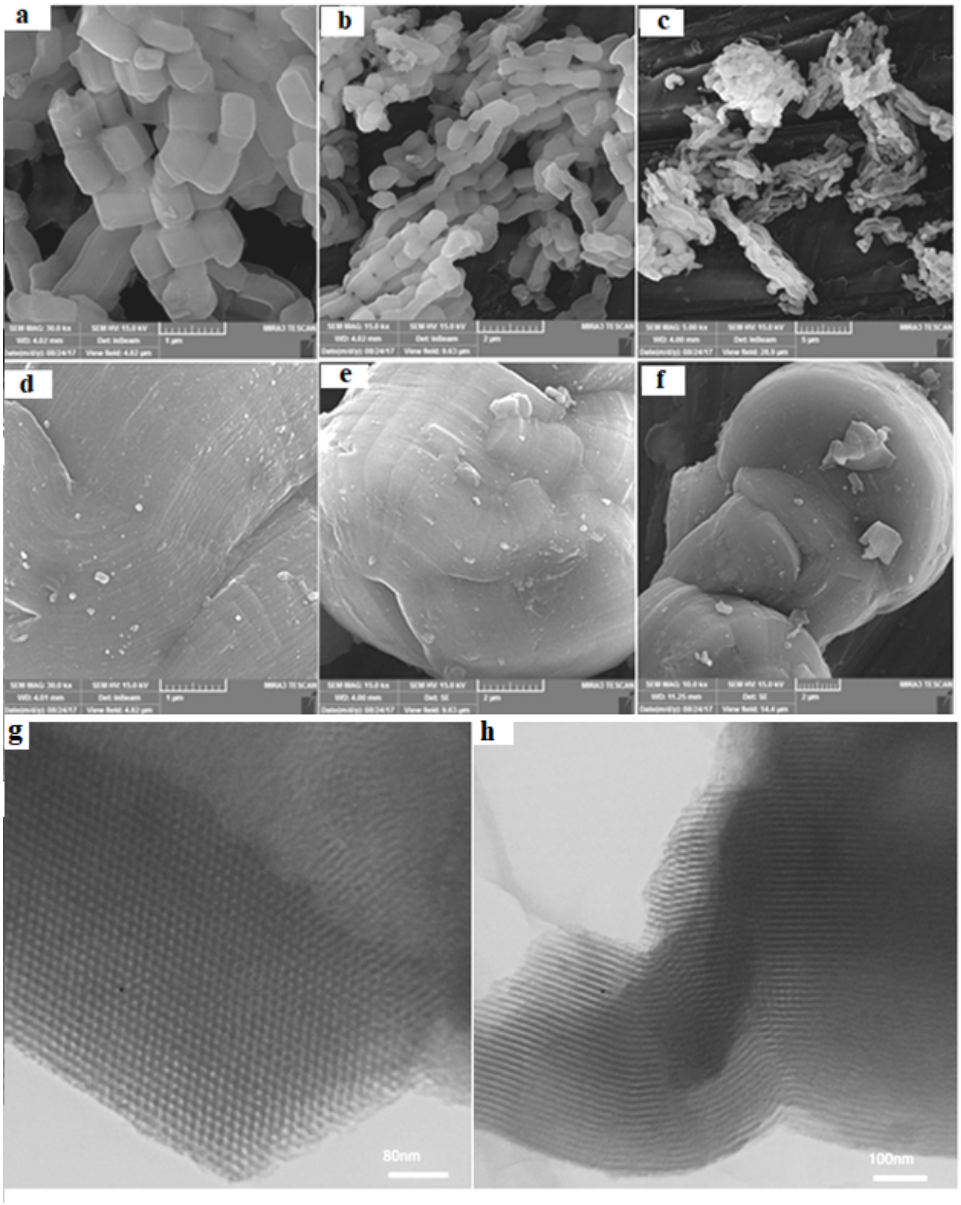

Fig 2. SEM images of SBA-15 (a,b,c) and NH2/SBA-15/NTAA (d,e,f), TEM images of SBA-15 (g) and NH2/SBA-15/NTAA (h)

167x207mm (96 x 96 DPI)

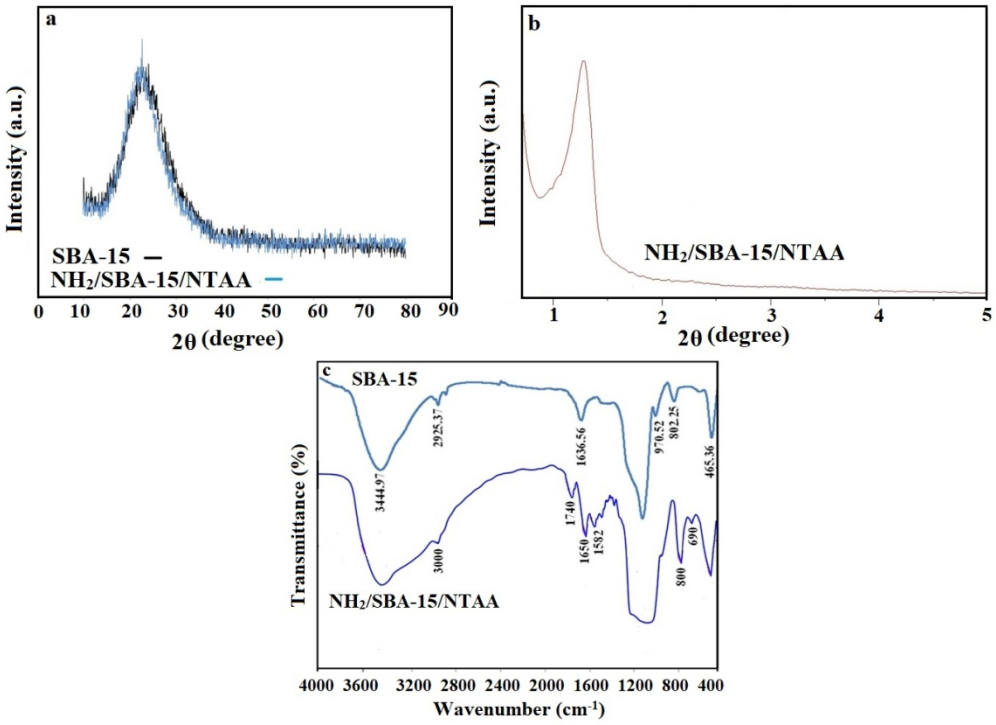

Fig.3. XRD patterns of the SBA-15 and NH2/SBA-15/NTAA at high angle (a), NH2/SBA-15/NTAA at low angle (b), FTIR spectra of SBA-15 and NH2/SBA-15/NTAA (c).

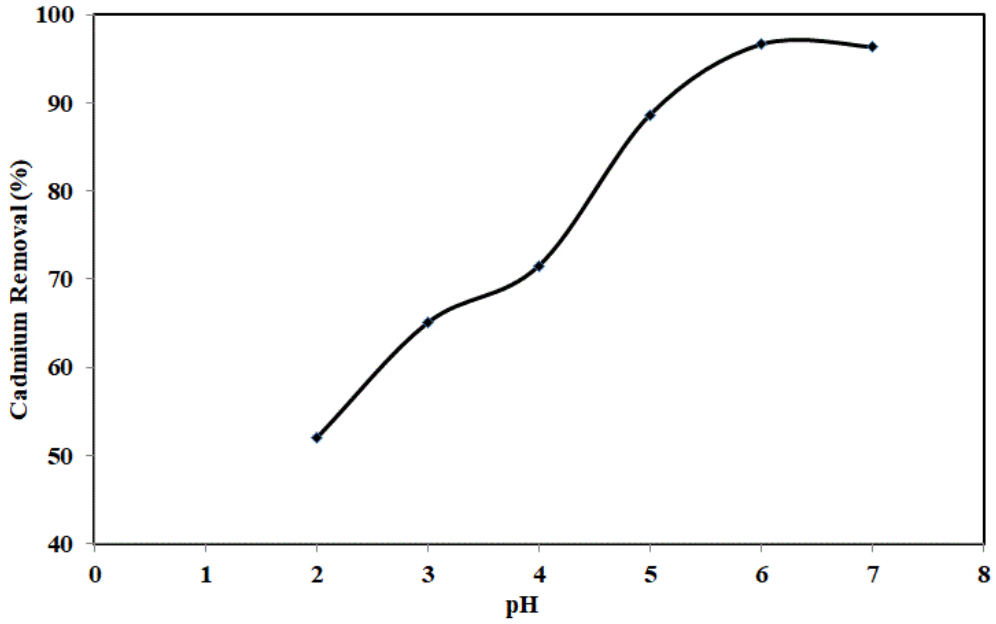

Fig.4. The effect of pH on the Cd+2 removal (adsorbent dosage: 250 mg/L, 60 ppm cadmium concentration, contact time of 60 min and T= 25°C).

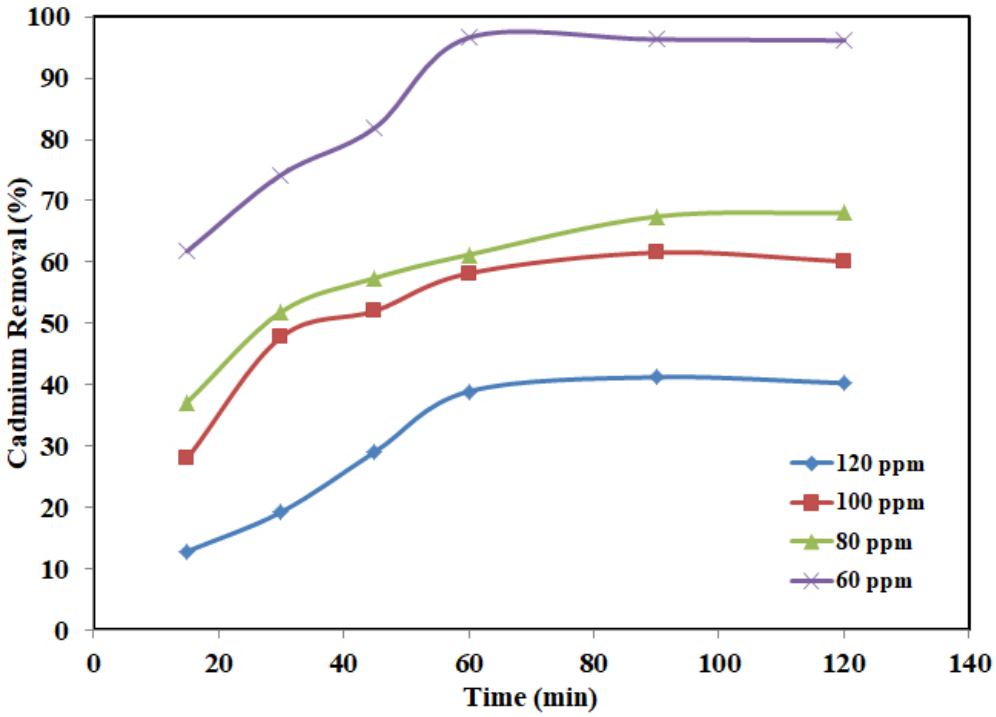

Fig.5. The effect of contact time on Cd+2 adsorption (cadmium initial concentration of 60 up to 120 ppm, adsorbent dosage: 250 mg/L, pH 6, and T= 25°C).

172x124mm (96 x 96 DPI)

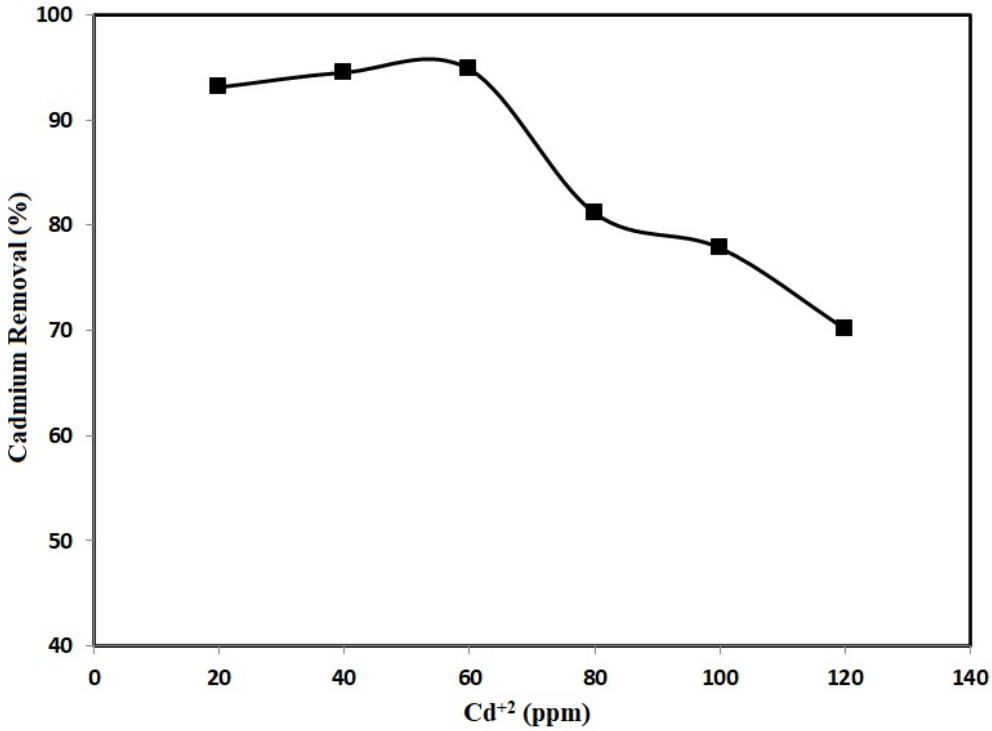

Fig.6. The effect of initial cadmium concentration on removal efficiency (adsorbent dosage: 250 mg/L, pH 6, contact time of 60 min and T= 25°C)

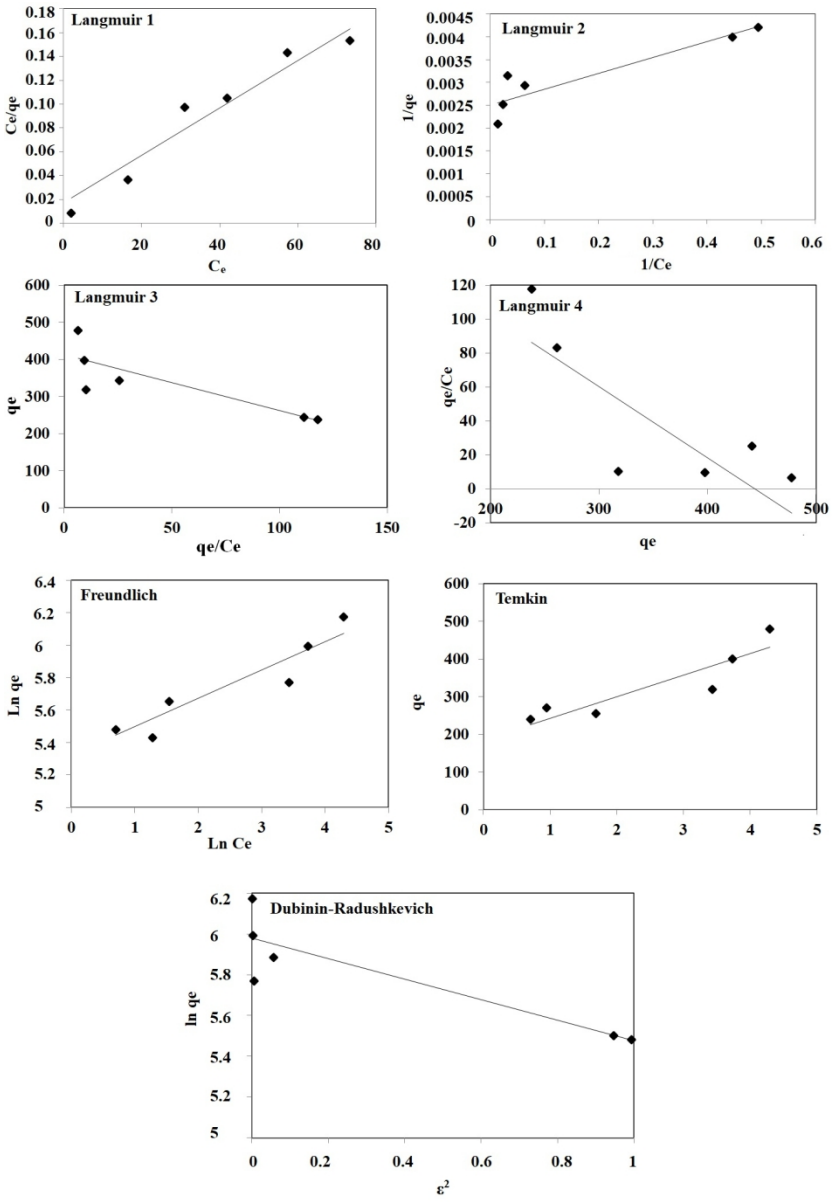

Fig .7. Adsorption isotherms of the Cd+2 adsorption at 25oC.

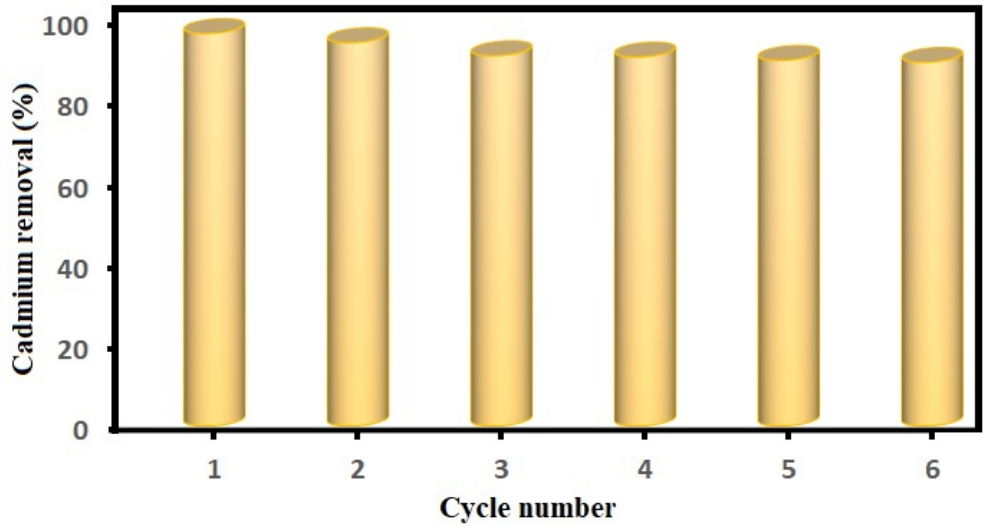

Fig.8. Reusability of NH2/SBA-15/NTAA (adsorbent dosage of 250 mg/L, initial cadmium concentration of 60 mg/L, contact time = 60 min at 25 oC).

Table 1. Characterization results of SBA-15 and NH_2/SBA-15/NTAA

Sample	[a]S_{BET} (m^2/g)	[b]Vp (cm^3/g)	[c]D_{BJH} (nm)
SBA-15	537.47	0.29	2.40
NH_2/SBA-15/NTAA	165.41	0.25	2.18

[a]Specific surface area, calculate from multi point BET analysis.

[b]Total pore volume.

[c]The pore diameter calculated from the adsorption part of the isotherm using the BJH method.

Table 2. Different isotherm parameters for adsorption of Cd^{+2} on NH_2/SBA-15/NTAA

Isotherm	*Linear form*	*Parameter*	R^2
Langmuir 1	$C_e/q_e=1/k_l\ q_m+ (1/q_m)\ C_e$ C_e/q_e vs. C_e	q_m=500 mg/g K_l=0.115 L/mg	**0.94**
Langmuir 2	$1/qe = 1/ k_l\ q_m Ce + 1/q_m$ 1/qe vs.1/Ce	q_m=400 mg/g K_l=0.714 L/mg	**0.80**
Langmuir 3	$q_e= q_m - qe/ k_L\ Ce$ $q_e$vs. q_e/C_e	q_m=411.73 mg/g K_l=0.668 L/mg	**0.63**
Langmuir 4	$q_e/C_e= q_m/k_l - q_e/k_l$ q_e/C_evs. qe	q_m=444.15 mg/g K_l=0.419 L/mg	**0.63**

Freundlich	$\ln q_e = \ln K_f + 1/n \ln C_e$ $\ln q_e$ vs. $\ln C_e$	n= 3.74 K_f=472.5 $(mg/g).(L/mg)^{1/n}$	**0.87**
Temkin	q_e vs. $\ln C_e$	B=57.734 J/mole A=24.361 L/g	**0.80**
Dubinin-Radushkevich	$\ln q_e = \ln q_m - \beta\varepsilon^2$ $\ln q_e$ vs. ε^2	q_m=395.44 mg/g β=0.504 E=8.996 kJ/mole	**0.70**

Table 3. Comparison of maximum adsorption capacity (q_m) for adsorption of Cd (II) by different adsorbents reported in the literature

Adsorbent	**q_m (mg/g)**	**Reference**
polyacrylic acid modified magnetic mesoporous carbon	406.60	52
Chitosan templated mesoporous silica	1.66	15
polyamidoamine dendrimer grafted magnetic graphene oxide nanosheets	435.85	46
Mungbean husk	34.85	68
Nano-hydroxyapatite	64.10	69
sulfonic acid functionalized nonporous silica microspheres	178.80	70
chitosan-based Hydrogel polyacrylic acid-based Hydrogel	234.11 192.23	65
activated carbon	119.41	66
enteromorpha prolifera biochar modified by chemical reagents	423	63

rice straw-derived biochar modificatied by amin	84.266	67
NH_2/SBA-15/NTAA	***500***	***This Study***

Table 4. Kinetics parameters of pseudo-first order, pseudo-second order and intraparticle kinetic models

Cadmium Concentration (mg/L)	$q_{e,exp.}$	***Pseudo-first order***			***Pseudo-second order***			***Intra-particle diffusion***		
		k_1***(1/min)***	$q_{e,cal.}$***(mg/g)***	R^2	k_2***(g/mg.min)***	$q_{e,cal.}$***(mg/g)***	R^2	k_p***(mg/g.min$^{0.5}$)***	***C(mg/g)***	R^2
60	231.89	0.03	128.12	0.99	0.00020	322.58	0.99	2.68	151.60	0.97
80	286.44	0.01	121.75	1	0.00007	285.71	0.99	2.32	65.66	0.81
100	346.57	0.03	126.18	0.98	0.00220	357.14	0.99	3.99	314.61	0.98
120	431.13	0.03	133.79	0.94	0.00180	434.78	0.99	5.11	389.92	0.95